International Journal of Engineering and Advanced Technology (IJEAT)
ISSN: 2249-8958 (Online), Volume-7 Issue-6, August 2018

Electromagnetic Waves Interaction with Cytoplasm and Membrane of the Outer Segment of the Rod Photoreceptor Modelled and Analysed on HFSS

Kennedy A. Iroanusi

Abstract: ***Horn antennas are widely used in ultra-wideband (UWB) applications, medical imaging devices, and radars and also in other wireless astronomical applications; the antennas are commonly used as a feeding antenna for satellite parabolic reflectors (Daniyan et al. 2014). The use of horn antennas in wide variety of application are based on two reasons; excellent radiation characteristics with good directivity, high gain, very low level voltage standing wave ratio (VSWR), wide bandwidth and it is very easy to fabricate mechanically (Singh 2011). In this paper; we will consider the design of a compact conical horn antenna designed for the visible light spectrum as an inner segment of a human photoreceptor and the outer segment of the photoreceptor is designed as a cascaded unit cells rather as an interwoven structure consisting of cytoplasm and membrane using HFSS. The unit antenna structure will be excited by plane wave and simulated to study the properties and the overall contribution of the photoreceptor's outer segment in hyperacuity of human visual system without considering the outer segment of the rods or cones separately. In the future, the three types of cones (Large, short and medium wavelength cones) and rods will be modelled, evaluated and the outcomes will be published.***

Index Terms: ***Aperture Antenna, Conical Horn Antenna, Bioengineering, Hyper Acuity, Photoreceptors.***

I. INTRODUCTION

The horn antenna flare or taper provides impedance matching between the circular waveguide and free space; the horn section of the antenna is also called an electromagnetic radio frequency transformer. The impedance matched by the flare is about 377 Ω (Daniyan 2014). The horn antenna has been designed to operate at the optical frequency band in hundreds of terahertz radiating electromagnetic waves with wavelengths from 360nm to 700nm. The source of the electromagnetic waves will be plane waves to mimic light rays reflected on objects at various distance(s) could be seen by the human eye; the proton of light carries detailed information the object in terms of colour, shape and texture. However, some of the signals may be weaker reaching the human eye. The six layered convex lens projects the information from a two dimensional (2D) inverted images on the back of the retina with more details at the fovea region aided by the large concentration of colour cones, line of sight and focal length.

Manuscript published on 30 August 2018.
***** Correspondence Author (s)
Kennedy A. Iroanusi, Department of Electrical & Electronics, Dudley College of Technology, Dudley, United Kingdom, E-mail: mr.iroanusi@gmail.com

The other contributing factors are the antenna element factor, array factor and the overall building blocks of the outer segment of the rod and cones. Therefore, to evaluate the intensity of the waves receive and the angle of impact Therefore, It is very important that the horn antenna is methodically and successfully designed to investigate the contribution of the cytoplasm and membranes. Horn antenna should be able to achieve a very good gain and directivity to deliver the incident electromagnetic signals to the multimode outer segment of the photoreceptors; whilst preventing waves radiating through undesirable modes at the waveguide section of the horn antenna (Daniyan 2014). The horn medium antenna will provide functions of a transmission medium at the inner segment of the photoreceptors provide the outer segment for light spectrum components as guided electromagnetic waves travelling in the waveguide. The broadcasted waves at the outer segment are for further signal processing as a receiving optical system. The dual mode feed horn for the cascaded unit cells provided excellent characteristics over the visible lights spectrum. It is essential that reflections and in terms of standing waves at the waveguide are minimised; therefore an optimum flare angle is used. It is essential to review the literatures involving biological materials properties, biomechanical, dielectric, and anatomic characteristics of the human eye before designing the cytoplasm and membrane on Ansys HFSS taken into consideration loss in vision. The factors affecting the optic nerves head (ONH), the anatomic, biomechanics properties contributes to the overall loss in retinal ganglion cell using finite element method with input factors using a computational eye modal with ocular tissues parameters, intraocular pressure and geometric dimension. The researcher's recorded intraocular pressure induced strain on glial cells, assisting ganglion cell axons; which contributes to loss in vision. The sensitivity analysis and geometrical input factors used of retinal thickness of 0.2mm baseline, but ranges from 0.16 to 0.24mm, optic nerves angle of 50^0, but ranges from 64 to 98^0. The Poisson ratio of the retina as 0.49 as baseline and ranges from 0.4 to 0.49, Young Modulus of the retina as 0.03MPa as baseline and ranges from 0.01 to 0.09 MPa) all as input factors. The output measurement determined the retina's peak Von- Mises stress from 0.62 to 4.04Kpa, peak maximum strain from 1.94 to 6.19 percent, mean strain of 0.54 to 2.77 percent (Sigal et al 2005). Some of biomechanical properties are essential for material design on HFSS.

Drago and Ridella researched on the evaluation of electric field components at any point inside a biological cell (Drago et al 1982). The work centred on the study of the electromagnetic difficulties associated to electric field study in non-homogenous material, but did not expand on the effects of electromagnetic waves on a biological material.

The work used significant published experimental, data available to generate various equations to achieve an equivalent model and Maxwell equations are required for solution. Cut –off wavelength, phase velocity, group velocity, modes in the waveguide region, field distribution configuration and finally attenuation are all essential in this type of study. The bio-electromagnetic properties of cytoplasm maybe studied and evaluated with some degree of accomplishment in the laboratory based on the peculiar and sensitive nature of the material in Human visual system (HVS). Researchers from the institute of biology at Humboldt University, in Berlin Germany; conducted a study on the dispersion of human cytoplasm using di-electrophoretic and electro-rotational evaluation approaches to measure the material properties such as the conductive and axial ratio of 1:2 at a wide frequency range from 2 KHz to 200 KHz, but did not reach the terahertz region. The cytoplasm conductance measured is 0.4 S/m at dielectric constant of 212 and capacitance of 9.97 mF/M with dispersion occurring at 15MHZ with material conductivity of 0.535 S/m and dielectric constant of 50 (Gimsa et al 1996:1). The determination of the dielectric characteristics are based on the predominant β-dispersion frequency band from 2 KHz to 200 MHz for the biological material, which helps in the estimation of the cytoplasm material capacitance, conductance and other related properties. As cytoplasm consists of very high level of proteins and the dispersion of the cytoplasm protein has been widely researched (Gimsa et al 1996:2). In the past, cytoplasm were treated as a homogeneous material comprising of haemoglobin suspension and cytoplasm ion characteristics; the dielectric dispersion is taken into account as the overall reduction of permittivity as frequency rapidly increases, which causes the proteins to fluctuate in the field for the dipole moment (Gimsa et al 1996:3). The conductivity of the material at Direct current (DC) level with the presence of sodium and potassium ion on the cytoplasm disks reaches up to 207mM in concentration. The laboratory researchers made many assumptions during the experimental measurement and obtained results through other laboratory methods. They hypothesized that the limitations in the concentration of haemoglobin, molecular mobility and the sensitivity of ions to haemoglobin; is based on the increase of ions as the cells decrease. The protein contributes to the overall dispersion of the cytoplasm characteristics as the torque is generated in the rotating electric field. At an increase in frequency (in the order of tens of MHz) results to an overall increase in displacement current, which contributes to the material conductivity, but the ionic mobility are negligible in rebounding (Gimsa et al 1996). The human body consist of various sensory systems packed with electrical pulses to enable the flow of data, interpretation of processed information and the control of the human body functionalities especially in the area of human vision, brain activities, various organ operations and human movement; pertaining to the movement of muscle, ligaments and fibres. These activities amounts to billions of electrical pulses generated from biochemical and electrochemical potentials with various sensory cells. These electrical pulses generated per minute are essential to medics; to acquire very important medical information on patients such as an electro-oculogram to measure eye response, electro-retinogram, electro-encephalogram for brain functions, and electro-cardiogram for heart response and electromyogram for muscle movement. The human central system controls the brain, the peripheral nerve such as the optic nerves, neurons for data transportation and ocular operations. The neuron network is very complex and there several interconnections providing a vast net of very useful information. This interconnection provides a small channel for photoreceptors communication in HVS; which explains the reason why the rod and cones work together in photopic vision and when several factors or die-off, the cones affect the rods will also starts dying off too. The researchers at Ohio State medical centre injected tracing molecules in the form of a glowing substance into the cones of a golden fish; which stayed in the cone of the retina during the day, but at night it migrated to other cones and rods; the channel exist around the neuron synapses. The neuron of the inner and outer segment of the photoreceptors known as the rod and cones consist of an unprotected or exposed nucleus for better sensitivity and the cell also consist of axons, mitochondria, synapses (Tobey 1975). The nucleus consist of the genetic DeoxyriboNucleic Acid (DNA) information of rod or cone and controls the operation of the overall cell as a receiving antenna based on the information it receives back from the cascade (few thousands) of interwoven pico-scaled optic disc known as the cytoplasm and membranes. The overall network of hexagonal layout of photoreceptors forms a complex phased array antenna with receiving nodes. The electromagnetic waves from light signals from a two dimensional view is converted from the natural plane wave into electrical pulses due to the synaptic firing. The overall 120 million photoreceptors will pass the information to one million optic nerves to transport data through the optical chiasm; the right eye information to the left brain and the left eye information to the right brain for data processing and the reformation of a two and half dimensional image (near 3D) in our brain. The electromagnetic signal radiating through the axon moves at speed range of 0.6 to 100m/s approximately (Tobey 1975), the outer segment membrane helps in the conduction based on electrical potential due to hyperpolarisation and depolarisation of the inner and outer segment of the photoreceptors resulting to more negativity or more positively charged sodium ions. The change in potential difference and the existence of ΔV from -40mV to -80mV and the existence of electric field between the inner and outer cellular fluids, but the resting potential is at -40mv. However, when there are no light stimulation or excitation received through the pupil, through different refractive indexes of different layers of the eye materials such as the anterior chamber, the six-layered convex lens, vitreous gel, inner segment of photoreceptors and several 150 Pico metre scaled outer segment cytoplasm and membrane. Nernst equation represents the equilibrium or relative ratio of positive or negative concentration in a cell

Published By:
Blue Eyes Intelligence Engineering
and Sciences Publication (BEIESP)

$$\frac{C_i}{C_o} = e^{-\frac{Z.e(V_i - V_o)}{K.T}}$$

K =Boltzmann constant = 1.38x10^{-23} J/K

Z = Value of ion

e = charge = 1.6 x 10^{-19}C

$\frac{C_i}{C_o}$ If it is interger represents positive ion, but if it is decimal fraction represents negetive ions

E is the Electric field [E = $\frac{\delta V}{\delta x}$ (V/m)]

δV is the potential difference

δx is the disc dimension in the x - direction

The dialectical constant (K) should be approximately equal to 7, the electrical permittivity of free space (ε_o) is 8.85 x 10^{-12} C^2/Nm^2. The accumulated charges (Q) at the surface (S) of the membranes and cytoplasm can be deduced as:

$$Q = k.\varepsilon_O.\varepsilon_m.S.E \quad (C/m^2)$$

The charge density of the materials $\frac{Q}{S} = \frac{C.V}{S}$

C= $\frac{Q}{V}$ and $\frac{C}{S} = \frac{K.\varepsilon_O.\varepsilon_m}{d}$ $\left(\frac{F}{m^2}\right)$

d is the cellular distance

There are leakage current (I) across the materials as it is not a perfect dielectric materials. The resistance offered to the follow of leakage current is R =$\frac{P.d}{S}$. The time response constant will be $\tau = R.C$.

(-I) =$\frac{-V}{R.C}$ and V (t) = $V_o.e^{-\frac{t}{\tau}}$

II. DESIGN OF ANTENNA

In waveguides involving dielectrics, there are three basic losses namely ohmic loss, dielectric losses and the critical breakdown losses. Current circulating the conductor's surface such as Perfect Electric Conductor (PEC) because of skin effect causes the ohmic loss. The dielectric losses occur when the insulator in between the waveguide is being heated up, but air has very low dielectric losses, but does not absorb significant reflections. The critical VSWR could damage the insulator inside or even the wall of the circular waveguide. Since the desired conical horn antenna will consist of a circular waveguide, it is essential we comprehend the microwave theorems behind the design of circular waveguide.

The design parameters are the radius, operating wavelength, maximum cut-off wavelength, and guide waveguide. The cylindrical waveguides will comprise of three coordinate systems (r,φ, z); the electromagnetic signals are kept inside the waveguide at a frequency slightly higher than the cut-off wavelength. In a multimode dispersion; the electromagnetic signals can propagate inside the waveguide in different modes with different time delay amongst the modes due to the arrangement of fields inside the waveguide and high attenuation could be achieved, but single mode does not allow dispersion. There are two common modes known as the Transverse Electric (TE or H modes) as the electric field in the direction of propagation (Z- direction) is equal to zero; therefore transverse and the magnetic field in z-direction is not zero. In Transverse Magnetic mode (TM or E mode), the magnetic field in Z-direction is equal to zero, but the electric field in Z-direction is not equal to zero. The dominant modes will be TE_{11} and TM_{01}. The field phasor for the TE mode can be expressed derivative and Bessel functions without $e^{-\propto z}$ representation.

The design coordinates (r,φ, z) are used to express electric field and magnetic components in those directions for TE mode are:

$$E_r = \frac{j\omega\mu m}{h^2 r} H_O Sin(m\varphi) J_m(hr)$$

The instantaneous $E_r$fields (e.g.$E_r.e^{j(\omega t - \beta z)}$) is

$$E_r(t) = \frac{-\omega\mu m}{h^2 r} H_O Sin(m\varphi) J_m(hr) \sin(\omega t - \beta z)$$

$$E_\varphi = \frac{\omega\mu}{h} H_O Cos(m\varphi) J_m(hr).\frac{\delta J_m(hr)}{\delta(hr)}$$

The instantaneous $E_\varphi$fields

$$E_\varphi(t) = \frac{-\omega\mu}{h} H_O Cos(m\varphi) J_m(hr).\frac{\delta J_m(hr)}{\delta(hr)} \sin(\omega t - \beta z)$$

$$E_z = 0 = E_z(t)$$

$$H_\varphi = \frac{j\beta m}{h^2 r} H_O Sin(m\varphi) J_m(hr)$$

The instantaneous $H_\varphi$fields

$$H_\varphi(t) = \frac{-\beta m}{h^2 r} H_O Sin(m\varphi) J_m(hr) \sin(\omega t - \beta z)$$

$$H_r = \frac{-j\beta}{h} H_O Cos(m\varphi) J_m(hr).\frac{\delta J_m(hr)}{\delta(hr)}$$

The instantaneous H_r fields

$$H_r(t) = \frac{\beta}{h} H_O Cos(m\varphi) J_m(hr).\frac{\delta J_m(hr)}{\delta(hr)} \sin(\omega t - \beta z)$$

$$H_z = H_O Cos(m\varphi) J_m(hr)$$

The instantaneous H_z fields

$$H_z(t) = H_O Cos(m\varphi) J_m(hr) \sin(\omega t - \beta z)$$

Whereby the Bessel function is related to the mth order ($J_m(hr)$)

$$\frac{\delta[J_m(hr)]}{\delta(hr)} = \left[\frac{m}{hr} J_m(hr) - J_{m+1}(hr)\right]$$

Chi= χ'_{11} is the nth zero root of mth order of Bessel function = 1.8412

The propagation constant is equal to $2\pi\sqrt{\mu\varepsilon f_c}$

$$\lambda_c = \frac{2\pi R}{\chi'_{11}}$$

Lowest Cut-off frequency

Published By:
Blue Eyes Intelligence Engineering
and Sciences Publication (BEIESP)

$$f_c = \frac{\chi'_{11}}{2\pi R\sqrt{\mu\varepsilon}}$$

However, normalised cut-off wavelength is

$$\frac{\lambda_c}{R} = \frac{2\pi}{\chi'_{11}}$$

Then Chi= χ'_{11} will be 3.4125.

The dominant in TM mode will be TM_{01}

In those directions for TM mode is:

$$E_\varphi = \frac{j\beta m}{h^2 r} E_O Sin(m\varphi) J_m(hr)$$

The instantaneous E_r fields

$$E_\varphi(t) = \frac{-\beta m}{h^2 r} E_O Sin(m\varphi) J_m(hr) \sin(\omega t - \beta z)$$

$$E_r = \frac{-j\beta}{h} E_O Cos(m\varphi) J_m(hr).\frac{\delta J_m(hr)}{\delta(hr)}$$

The instantaneous E_r fields

$$E_r(t) = \frac{\beta}{h} E_O Cos(m\varphi) J_m(hr).\frac{\delta J_m(hr)}{\delta(hr)} \sin(\omega t - \beta z)$$

$$E_z = E_O Cos(m\varphi) J_m(hr)$$

The instantaneous E_z fields

$$E_z(t) = E_O Cos(m\varphi) J_m(hr) \sin(\omega t - \beta z)$$

$$H_r = -\frac{j\omega\varepsilon m}{h^2 r} E_O Sin(m\varphi) J_m(hr)$$

The instantaneous H_r fields

$$H_r(t) = \frac{\omega\varepsilon m}{h^2 r} E_O Sin(m\varphi) J_m(hr) \sin(\omega t - \beta z)$$

$$H_\varphi = \frac{-j\omega\varepsilon}{h} E_O Cos(m\varphi) J_m(hr).\frac{\delta J_m(hr)}{\delta(hr)}$$

The instantaneous H_φ fields

$$H_\varphi(t) = \frac{\omega\varepsilon}{h} E_O Cos(m\varphi) J_m(hr).\frac{\delta J_m(hr)}{\delta(hr)} \sin(\omega t - \beta z)$$

$H_z = 0 = H_z(t)$

Chi= χ'_{01} is the nth zero root of mth order of Bessel function = 2.4049

The propagation constant is equal to $2\pi\sqrt{\mu\varepsilon f_c}$

$$\lambda_c = \frac{2\pi R}{\chi'_{01}}$$

Lowest Cut-off frequency

$$f_c = \frac{\chi'_{01}}{2\pi R\sqrt{\mu\varepsilon}}$$

However, normalised cut-off wavelength is

$$\frac{\lambda_c}{R} = \frac{2\pi}{\chi'_{01}}$$

Then Chi= χ'_{11} will be 2.6127

.

Guide wavelength can be calculated using the formulae below:

$$\lambda_g = \lambda.\left[1 - \left(\frac{\lambda}{\lambda_{c,11}}\right)^2\right]^{-\frac{1}{2}} \quad \text{or} \quad \lambda.\left[1 - \left(\frac{\lambda}{\lambda_{c,01}}\right)^2\right]^{-\frac{1}{2}} \text{or} \lambda.\left[1 - \left(\frac{f}{f_{c,11}}\right)^2\right]^{-\frac{1}{2}} \text{or} \lambda.\left[1 - \left(\frac{f}{f_{c,01}}\right)^2\right]^{-\frac{1}{2}}$$

There are changes in field in a sinusoidal fashion along z-direction with a phase velocity and group velocity as electromagnetic signals propagate in a zigzag pattern.

$$V_p \geq [\mu\varepsilon]^{-\frac{1}{2}} = \lambda_g.f$$

$$V_g \leq \frac{\lambda}{\lambda_g}.[\mu\varepsilon]^{-\frac{1}{2}}$$

The waveguide propagation constant are expressed as:

$$\beta_{11\,or}\,\beta_{01} = k.\left[1 - \left(\frac{\lambda}{\lambda_{c,11}}\right)^2\right]^{-\frac{1}{2}} \quad \text{or} \quad k.\left[1 - \left(\frac{\lambda}{\lambda_{c,01}}\right)^2\right]^{-\frac{1}{2}} \text{or} k.\left[1 - \left(\frac{f}{f_{c,11}}\right)^2\right]^{-\frac{1}{2}} \text{or} k.\left[1 - \left(\frac{f}{f_{c,01}}\right)^2\right]^{-\frac{1}{2}}$$

When the frequency (f) exceeds the antenna cut-off frequency ($f_{c,11}$ or $f_{c,01}$); then $\beta_{11\,or}\,\beta_{01}$ will be considered as real. Therefore, $e^{j\beta_{11}^z}$ may lead to a phase shift on the expected result. However, the cut-off frequency is larger than frequency then $\beta_{11\,or}\,\beta_{01}$ is imaginary and the electromagnetic signal is attenuated at the source.

The attenuation constant is represented as:

$$\alpha_{c,11}^{TE} = \frac{R_s}{\rho\eta}.\left[1 - \left(\frac{{f_{c,11}}^{TE}}{f}\right)^2\right]^{-\frac{1}{2}}.\left[\frac{m^2}{(\chi'_{11})^2 - m^2} + \left(\frac{{f_{c,11}}^{TE}}{f}\right)^2\right]$$

$$\alpha_{c,01}^{TM} = \frac{R_s}{\rho\eta}.\left[1 - \left(\frac{{f_{c,11}}^{TM}}{f}\right)^2\right]^{-\frac{1}{2}}$$

R_s is surface resistance = $(\sigma_c\delta)^{-1}$

δ is the skin depth = $(\mu f\pi\sigma_c)^{-\frac{1}{2}}$

σ_c is conductivity (S/m)

The bandwidth of a single mode is the ratio of TM to TE mode; which is $\frac{2.4049}{1.8412}$ to yield 1.3062:1 bandwidth.

The power absorbed by materials can be determined by:

$$P = \frac{\pi^2 B_p^2 d^2 f^2}{6.\rho.k.D}$$

P = Power loss or absorbed by material per mass (W/Kg)

d = thickness (m)

B_p is the peak magnetic field (T)

K is contant

ρ is resistivity (Ωm)

D is the density in Kg/m^3

Published By:
Blue Eyes Intelligence Engineering and Sciences Publication (BEIESP)

A. Physical Model

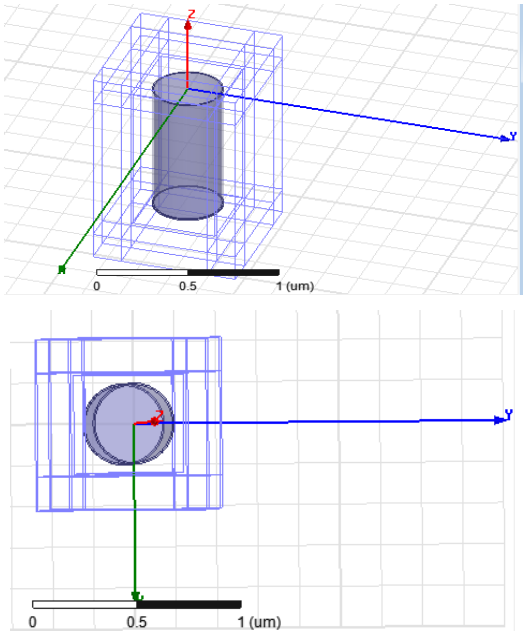

Figure 2: Top View of Waveguide

A. Modes of the Waveguide

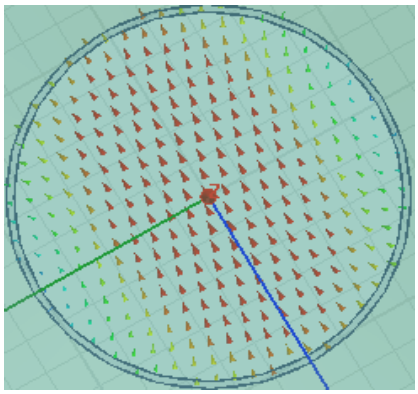

Dominant TE_{11} mode

Figure 3. TE Mode

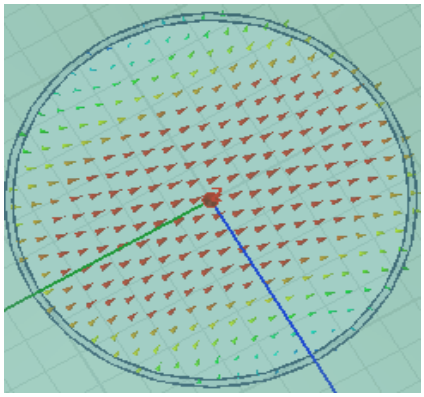

TM_{01} mode

Figure 4: TM Mode

The conical horn antenna is designed based on the Horn antenna formulas below:

The diameter of the conical horn aperture can be determined using the formula below.

$$d = 2a = 3.L.\lambda$$

Whereby, the waveguide aperture is denoted as "a".

The length of the horn, not the aperture size, affects the gain of the conical horn antenna. The gain of the horn antenna can be determined by utilising the gain formula below.

$$G = \frac{\pi^2 . d^2 . E_a}{\lambda^2}$$

Whereby, d is the diameter of the horn aperture in micro-metres (µm), λ is the wavelength in Nano-metres (nm), L is the slant length, A is equal to the aperture area in μm^2 , π is a pie or constant equivalent to the ratio of $\frac{22}{7}$ and E_a is the dimensionless factor between 0 to 1 known as aperture efficiently. The typical range for E_a should be within the range of 0.4 to 0.8; most published journals estimated it to be 0.522 for horn antenna optimisation and has a directed linkage with overall field distribution (Daniyan 2014). The electromagnetic waves radiating through the waveguide accelerates at the speed of light with minimum reflections, but some electromagnetic waves travels faster than others do. It is essential to determine the cut-off frequency of the waveguide.

The antenna cut-off frequency is directly proportional to the radius of the circular waveguide as shown below;

$$\lambda_L = 3.412.R$$

The speed of visible light is related to the permittivity, permeability, refractive index, frequency at which an electromagnetic wave travels, energy stored or absorbed in a synthetic dielectric material and the mass of any material using the formulas below:

$$C = \frac{1}{\sqrt{\varepsilon_O \mu_O}} = f.\lambda = f.\eta = \sqrt{\frac{E}{m}} = \sqrt{\frac{E.\lambda}{h}}$$

C is speed of light through space = $299792458\ m/s$

f = frequency in THZ

η = Refractive index $\eta = \left(\frac{C}{C_m}\right)$

C_m = Speed of Light through material

ε_O = Permittivity of free space ($8.85419x\ 10^{-12}\ F/m$)

E = Energy in Joules

λ = wavelenth in nm

μ_O = Permeablitiy of free space ($4\pi\ x10^{-7} H/m$)

h = Planck's constant

m = mass in Kg

To deduce the highest and lowest frequency of operation will be:

$$f_H = \frac{C}{\lambda_L} = \frac{299792458}{390\ x\ 10^{-9}} = 769\ THz\ or\ 769000GHz$$

$$f_L = \frac{C}{\lambda_H} = \frac{299792458}{700\ x\ 10^{-9}} = 428.3\ THz\ or\ 428300GHz$$

The wavelength (λ_{cw}) of the electromagnetic waves inside the circular waveguide region of the horn antenna can be determined as:

$$\lambda_{cw} = \left[\left(\frac{1}{\lambda_o}\right)^2 + \left(\frac{1}{\lambda_L}\right)^2\right]^{-\frac{1}{2}}$$

While λ_o is the wavelength of free space and can be calculated as $\lambda_o = \frac{C}{f_{L_L}}$

f_{L_L} is a much lower frequency than the calculated f_L

Published By:
Blue Eyes Intelligence Engineering
and Sciences Publication (BEIESP)

Therefore, the circular waveguide length can be determined as:

$$L_{cw} = \frac{3.\lambda_{cw}}{4}$$

The horn antenna waveguide radius is determined to 0.25 μm, the waveguide length is deduced to be 0.5 μm, the wall thickness is 0.01 μm, the horn radius has been calculated as 0.69 μm and the horn length is determined as 0.99 μm.

III. MATERIAL CREATION AND ASSIGNMENT USING DEBYE DESIGN APPROACH (SYNTHETIC DIELECTRIC MATERIAL)

The cytoplasm and membrane of the photoreceptors are biological materials, which are frequency dependent with characteristics of a lossy dielectric in nature; the optical permittivity and conductivity at low frequency is required. The simulation analysis setup can only use either the interpolating or the discrete sweep to analysis the materials, but the fast sweep cannot be used based on the boundary conditions; the material is analysed at the centre frequency only.

Debye's relaxation polarization model:

$$\varepsilon_{r\_complex} = \varepsilon_{r\_optical} + \frac{\left(\varepsilon_{r\_static} - \varepsilon_{r\_optical}\right)}{j\omega\tau + 1}$$

The dielectric constant and the conductivity is expressed as:

$$\sigma = \sigma_0 + \frac{\omega^2 \varepsilon_0 \tau \left(\varepsilon_{r_{static}} - \varepsilon_{r_{optical}}\right)}{(\omega\tau)^2 + 1}$$

Whereby

σ is conductivity

τ is relaxation time.

ε_{r_static} is static or DC permittivity.

$\varepsilon_{r\_optical}$ is optical permittivity or highest frequency

This model is valid from microwave region up to the optical frequency region and the highest frequency used in this research.

$$\sigma_0 = \omega_1 \varepsilon_0 \varepsilon_r tan\delta_1$$

$$\sigma_2 = \omega_2 \varepsilon_0 \varepsilon_r tan\delta_2$$

Since the highest optical frequency is known; therefore the Debye's model requires the calculation of the relaxation time.

$$\tau = \frac{\omega^2 \varepsilon_0 \left(\varepsilon_{r_{static}} - \varepsilon_{r_{optical}}\right)}{\sigma_2}$$

All of the required parameters can be deduced using the equations above to achieve a Debye model of the lossy dielectric material for cytoplasm and membrane disc layers. Biological materials have similar properties to dielectric materials; the dielectric constant and permeability will be dependent on frequency at a point during simulation at very high frequency, which are rapidly changing leads to dispersion. The permittivity is also frequency dependent. Let the electric field be E = E $(x)\, e^{-iwt}$. The electric field diffusion on dielectric material can be represented as:

$$-eE(x, t) = m\ddot{x} + m\gamma\dot{x} + m\omega_o^2 x$$

Taking into consideration that effects of magnetic components are limited and there are very small magnitude of oscillations. Hence the electric dipole (P) is equal to N_P number of molecules or equal to $\varepsilon_o . \chi_e . E$. The following symbols on the equation above are Chi of an electron notation (χ_e), gamma(γ), e is electron, x is x-direction, t is time, m is the mass and E is the Electric field.

In each of the unit theme designed; there will be several number of electrons per unit molecule; with fraction number of electrons binding to the material at a binding frequency (ω_{io}) and damping factor $(y_i i)$. It is important to note that the binding of electrons on the material will not be the same all over the material. The dipole constant can be represented as:

$$\varepsilon_m = \frac{\varepsilon}{\varepsilon_0} = 1 + \chi e$$

The overall dipole moment can be represented as:

$$P = \left[1 + \frac{Ne^2.}{m\varepsilon_o}\left(\sum \frac{d}{(\omega_{io}^2 - \omega^2 - i\omega\gamma_i)}\right)\right]$$

The overall dipole can be expressed in mathematical form above is linked to the resonant absorption and abnormal dispersion of biological material. The real and the imaginary parts of clear absorption of fields the irregular dispersion. We need to start with the total permittivity of the material represented as

$$\varepsilon = \left[\varepsilon_0 + \frac{Ne^2.}{m}\left(\sum \frac{d}{\left(\frac{\omega_{io}^2}{\omega^2} - 1 - \frac{i\gamma_i}{\omega}\right)}\right)\right]$$

For ω is more than ω_{io}, then $\varepsilon \approx \varepsilon_o - \frac{Ne^2.}{m\omega^2}\sum d$

The real permittivity can be represented as:

$$\varepsilon_{RE} = \left[\varepsilon_0 + \frac{Ne^2.}{m}\left(\sum \frac{d\,(\omega_{io}^2 - \omega^2)}{\left((\omega_{io}^2 - \omega^2)^2 + \omega^2\gamma_i^2\right)}\right)\right]$$

The imaginary part of permittivity will be:

$$\varepsilon_{IM} = \left[\frac{N.e^2.\omega}{m}\left(\sum \frac{d.\gamma_i}{((\omega_{io}^2 - \omega^2)^2 + \omega^2\gamma_i^2)}\right)\right]$$

At higher frequency, the damping constant will be higher but at lower frequency, it will be negligible. At very high frequency, the permittivity of material may be significantly lower than the permittivity of free space; tends towards negative value. At higher frequency (at solution time), the imaginary part will reach its peak resonant in the permittivity; thus will cause the material to absorb energies from the fields affecting it.

A. Incident Plane Wave

The plane wave propagates along the Z- direction with field's perpendicular to Z- direction. The radiation boundary is used for weak scattering problems as a scattered field, else a total field formation in the form of incident field with reference to Frequency Selective Surfaces for resonant materials. The default plane wave as Cartesian vector input type was selected for excitation. The plane wave can be setup in a Cartesian format and could be modelled as

$$\vec{E} = \vec{E}_O e^{-j\vec{k}.\vec{r}} .= \sqrt{\frac{\mu_O \mu_M}{\varepsilon_O \varepsilon_M}} . H.\vec{r}$$

Whereby $\vec{k} = k\hat{k}$ and k is wave number of the global background material for regular/propagating plane waves.

Published By:
Blue Eyes Intelligence Engineering
and Sciences Publication (BEIESP)

$\vec{r}$ is the radial coordinates of source or field point

$\hat{k}$ for evanescent waves since they do not depend upon the background global material. The Farfield of the material will be calculated using the Green function and intrinsic impendences of the materials to compute it. The overall electric field can be modelled using the coordinates E(x, y and z) as:

$$E(x, y, z) = \int \left((j\omega\mu_o H_{tan}) G + (E_{nor}.\nabla G) + (E_{tan}.\nabla G) \right) \delta s$$

Whereby G is the free space Green function

$$G = \frac{e^{-jk_o|r-r'|}.\sqrt{\varepsilon_m \mu_m}}{|r-r'|}$$

j is imaginary notation equal to $\sqrt{-1}$

ω is angular frequency in rad/s

$E_{tan}$is electric field components tangent to surface of material

E_{nor} is an electric field component normal to material

H_{tan} is magnetic field components tangent to material

ε_m is the relative permittivity of material

μ_m is the relative permeability of material

r and r' is field point and source of material

The plane wave from the source reaching the cytoplasm and membrane in the z-direction can be modelled as:

$$C_m = \beta + \frac{1}{2} i\alpha = \left[\mu_o \varepsilon_o \left(\frac{\varepsilon_{RE} + \varepsilon_{IM}}{\varepsilon_o} \right) \right]^{\frac{1}{2}}$$

The electric field (E) is $E = \varepsilon . e^{\left[-\frac{1}{2}\alpha z\right] + [-i\beta z - i\omega t]}$ and the overall intensity changes rapidly as the square of electric field changes and decays $e^{[-\alpha z]}$. Whereby α is the attenuation constant; the attenuation is not homogenous all over the material; we will assume that the biological material lowest resonant frequency (ω_{io}) should be more than zero as a non-conductor. The plane ware hormones acting on the field and the material dielectric constant can be represented using Maxwell's equation as:

$$J = \sigma E = \nabla X H - \frac{\delta \varepsilon_m E}{\delta t} = -i\omega \left(\varepsilon_m + \frac{i\sigma}{\omega} \right) E = -i\omega\varepsilon E$$

Field Plot (Magnitude Electric Field acting on material in V/m)

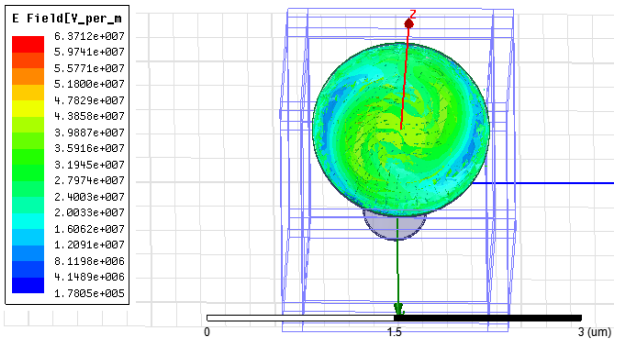

Figure 5: E Field Post Process Simulation of Biological Material

Note: There is also a complex Electric field plot of not added in this thesis

B. Field Plot (Magnitude Magnetic Field Acting on Material in A/m)

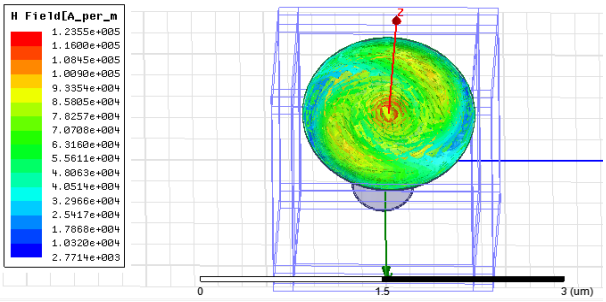

Figure 6: H-Field Post Processed Simulation on Biological Material

C. Field Plot Jvol (Acting on Biological Material in A/m^2)

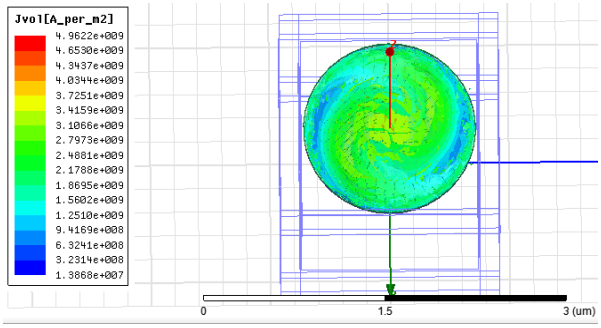

Figure 7: JVOL Post Processed Simulation on Biological Material

However, there is a direct link between dielectric constant of the biological materials based on its individual dielectric constants and the radiating conductor. We can assume that the cytoplasm and the membrane of the photoreceptors are made up of molecules, atoms, and ions dipoles with some bounded atoms, at the point of the electric field is applied through the horn antenna aperture; it will cause the electrons to be excited to move slightly because of the nature of the material. However, the electric current density (J) is directly proportional to the product of the conductivity (σ) proportionality constant and the electric field (E). The conductivity is the measure of how reluctant or how quick an electron moves about the material. The conductivity can be expressed as a mathematical quantity; which is equal to the product of charge and electron mobility through the material as shown below:

$$\sigma = -q\mu$$

Whereby, q is the charge and μ is known as electric mobility.

The electric flux density is the product of permittivity with the applied electric field. The material consists of two components of electric current density within the biological materials known as an impressed electric current density and conduction current density of the horn antenna.

$$\nabla X \vec{H} = \left(\vec{J}_i + \vec{J}_c \right) + j\omega \vec{D}$$

The specific absorption ratio relates to the dissipation of power in a specific area in direct relationship with the static conductivity at an instantaneous occurrence, the polarisation loss inherent in the biological material ensures a non-zero imaginary permittivity.

Published By:
Blue Eyes Intelligence Engineering
and Sciences Publication (BEIESP)

The plasma frequency of the material depends on the overall quantity of electrons will be represented as:

$$\omega_p = \left[\frac{N.e^2}{\varepsilon_o m}\sum d\right]^{\frac{1}{2}}$$

The attenuation coefficient, the permittivity, permeability, the refractive index are all functions of frequency.

IV. THE ANTENNA MODEL

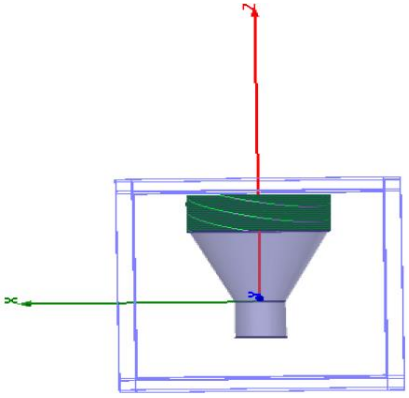

Figure 8: Cascaded Unit Cells Model (Antenna Element)

The HFSS software is analogues to a setup in anaerobic chamber for antenna measurement; the test antenna (TX) connected to the output of network analyser to be fed and allowed to transmit electromagnetic signals based on the operating wavelength and the receiving antenna with known characteristics. A half-wave dipole antenna is usually used as the receiving (RX) antenna and connected on the input of the network analyser ;whilst the walls of the anaerobic chamber performs the work of a boundary condition to minimize the simulation within the test environment and thereby minimising the overall simulation time. The measurement of the test antenna's radiation loss is achieved by calibrating the system for 0 dB insertion loss, the antenna starts at angle of 0° and the antenna's characteristics is measured, and the rotated at angle of 30° and the signal is measured again from the receiving antenna (Dipole antenna). An increment of 30° at each time to measure the signal gain in decibel (dB) until a 360° is reached. The angle in degrees is plotted with its corresponding measured electromagnetic signals in decibels obtained from the receiving (RX) antenna; the plot is presented in polar plots, smith charts, one dimension, two dimension, and three dimension plots.

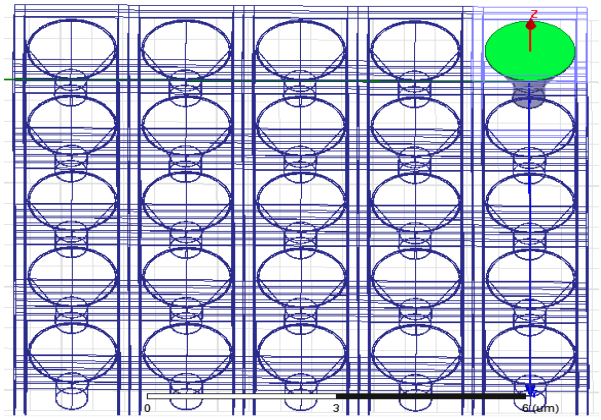

Figure 9: Array Element model

V. SIMULATION RESULT

A. Farfield Return Loss

The figure below implies that the antenna radiates best at 400THz, where S11 is equal to -20 dB and at 730THz, where S11 is -28dB. Further, at 360 THz the antenna will radiate very little, as S11 is nearer to 0 dB. Therefore, most of the power is reflected at that frequency point. The visible light spectrum starts at 430THz; for the behaviour of a rod sensor in the retina simulated on HFSS Ansys suggest that it radiate less at the beginning of the white light band and radiates more towards the end encompassing all colours making up the visible light spectrum maybe as a result of a loss emanating as a result of discontinuities of refractive index.

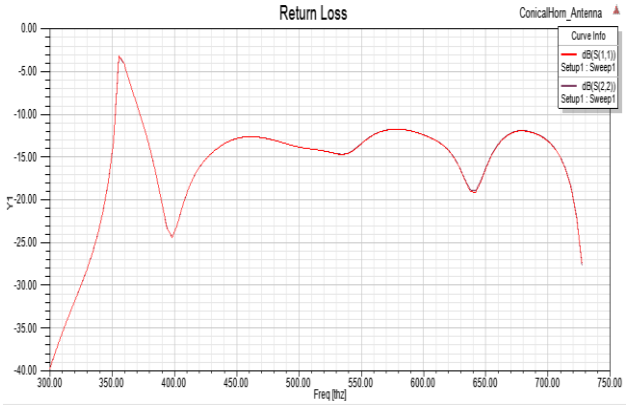

Figure 10: Return Loss for Test Antenna

The antenna shows a typical characteristics of a narrow band at the S11 at frequencies of interest did not go beyond -20dB for 20 percent of the entire bandwidth indicates a narrow-band; as the S11 did not go beyond -20dB at 20 percentage of the frequency range from 430THz to730THz.Low data rate due to narrow bandwidth.

B. Input Impedance

The load impedance is represented as the load impedance connected to a generator as a means of proving a voltage source for the antenna and the source has its associated source impedance (ZS) through a transmission line of length (L) and characteristic impedance (Z0). The input impedance could be found with the equation below with parameters such as the distance (L) from the load (ZL).The input impedance (Zin) is deduced with a distance (L) down the transmission line on the Smith Chart. The equations below corresponds to the points on the input impedance represented on the smith chart. The normalized load impedance is achieved by diving the load impedance (ZL) by characteristic impedance (Z0).

$$Z_{in} = \boldsymbol{Z_0}\frac{(\boldsymbol{Z_L} + \boldsymbol{jZ_0 tan\beta z})}{(\boldsymbol{Z_0} + \boldsymbol{jZ_L tan\beta z})}$$

Published By:
Blue Eyes Intelligence Engineering
and Sciences Publication (BEIESP)

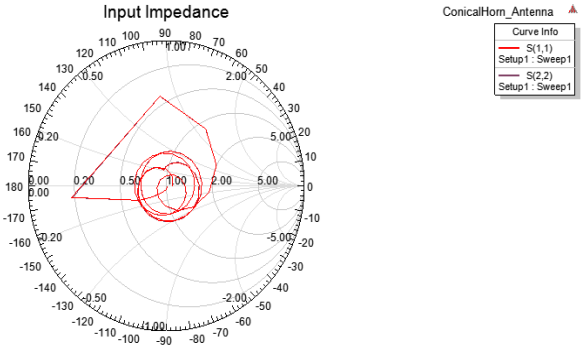

Figure 11: Input Impedance of the Test Antenna

Note: On the Smith Chart; proceeding towards the antenna, which is the load impedance corresponds to anticlockwise movement on the Smith Chart, while advancing towards the transmitter and/or receiver or generator corresponds to a clockwise rotation

C. Circular Polarisation

Electromagnetic wave performs behaves as a two-dimensional transverse wave and the circular polarization of an electromagnetic wave occurs when the electric field of that electromagnetic wave has a constant magnitude but its direction rotates with a specific time frame at a constant rate in a plane perpendicular to the direction of the wave. The electric field vectors determine the electrodynamic nature of the propagating wave in terms of its strength and direction. The circularly polarization is normally in one of two states; the right circular polarization in which the electric field vector rotates in a right-hand sense with regards to the propagation direction and/or left circular polarization in which the vector rotates in a left-hand principle.

The left or right hand polarized light wave could reverse, if it is reflected off a surface at normal incidence; which causes the rotation of the polarization plane to be the same as incident field known as the right handed circular polarization. While for the incident beam is referred to as the left-handed circular polarization for propagation in the reverse direction. The reflection associated to a dielectric at non-normal incidence is slightly different, as the dielectric does not have the same properties of the plain surface; therefore it will reflect the light at an angle beyond the Brewster angle, which means that the right circularly polarized light will reflect at grazing incidence emanating as slightly elliptical in nature.

3D Right Hand Circular Polarisation

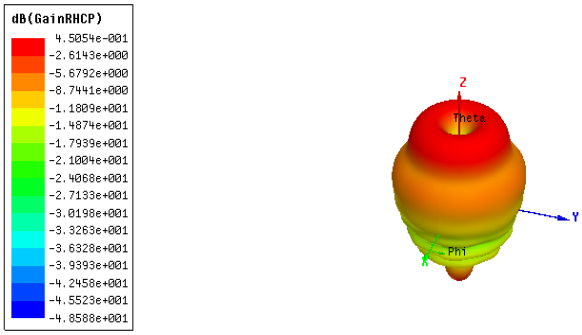

Figure 12: 3D Right Hand Circular Polarisation

D. Radiation Pattern (Polar Plot)

The arrow on the polar plot indicates the direction of maximum gain in dB, which is towards the 0° angle. The intercept of the -3dB line cutting the Gain (dB) polar plot and could be traced to the centre of the polar plot; the arc indicates the beam width. The front to back ratio is measured based on 0° and 180° points of the Gain (dB) plot. The shape and size of the antenna is a function of its purpose. The electromagnetic waves radiates outwards in all directions from the source as a travelling wave in the order of one cycle of the wavelength. Once the test antenna is fed, an electron flow will be setup within it with maximum concentration in one direction and reverses to the opposite side. The frequency determines the switching behaviour due to fluctuating magnetic field; as the electron field reverses, then the magnetic field is at its maximum with electric field at its minimum, the lines of force collapses and at the point of its flow reversal, the lines of force is at a specific direction. At the point, the field reaches its maximum and the lines of force will be on the opposite direction, the magnetic field reverses its direction every half cycle and the magnetic component is known as H-field, which indicates the strength of the field is equal to the amplitude of current standing wave. The amplitude of the current standing wave maybe 90° out of phase from the voltage standing wave. At any point, where the current is its maximum, it will be accompanied by a negative voltage and vice versa (voltage is at its maximum, it will be accompanied by a negative current) and therefore an electric field is created. When the polarity (voltage) changes, the direction of the electric field alternation; the electric field build-up towards the maximum at the opposite direction (negative polarity) also known as E-field. The E-field and H-Field builds up and collapse 90° out of phase with each other and constitutes the antenna's immediate field. It produces the radiation pattern propagating outwards with the vertical lines indicating the H-components and the horizontal lines indicating the E-components; each of the peaks creates a time-phase space quadrature between the peaks of the aforementioned components. The plane of E field determines the polarity of the antenna; in order to achieve a maximum signal, both the transmitting antenna and the receiving antenna must be on the same E-field plane. The H-field, E - field and the direction of propagation are perpendicular to each other in a corkscrew action. When the direction of propagation reaches a plain solid surface, the E-field and the direction of propagation reverses upon interaction with reflecting material and the direction, but the H-field stays in the same direction; which is in accordance with pointing rule. This is the same for pair of vectors, the signal strengths are sampled from various points in a geographical manner, and points of equal strengths can be drawn to achieve contour lines. The shape of the field from a radiating antenna with a fixed radius applied; a sectorial presentation. The vectors represent the strength and propagation of the signal; therefore a three dimensional representation is achieved and could be represented on a polar plot by sketching the tip of the vector lines; which aids towards the complete visualisation of the radiating characteristics.

Published By:
Blue Eyes Intelligence Engineering
and Sciences Publication (BEIESP)

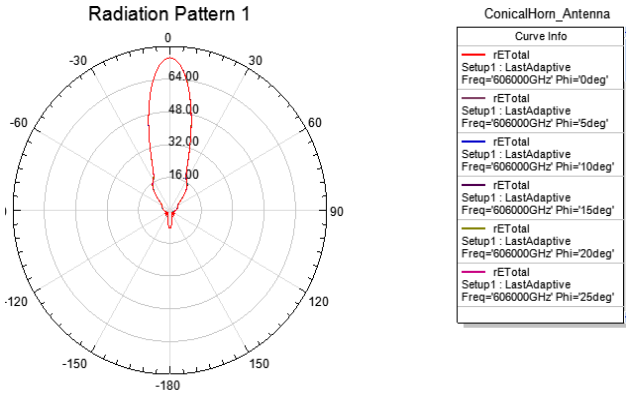

Figure 13: Radiation Pattern polar plot for Test Antenna

The maximum direction of the radiation pattern plot is towards the zero degrees and the plot shows some level of back-lobe due to reflections, slightly more than that of Horn antenna on its own. The overall gain exceeds 64dB.

E. Voltage Standing Wave Ratio against Frequency

It is essential to note that the electromagnetic radiation within the visible light spectrum that a typical human eye will respond are from 390nm to 700 nm wavelengths ;which in terms of frequency corresponds to a band in the vicinity of 430THz to770 THz. Therefore, the voltage standing wave ratio will be considered from the frequency of interest. However, it also good to know the wider VSWR behaviour of the antenna designed. A voltage standing wave ratio of 1:1 is desirable, but as the test antenna has shown a VSWR beyond two; indicating that reflected signal mixes with the incident signal resulting to power loss at that specific frequency. The practical approach towards the determination of Voltage Standing Wave Ratio (VSWR) is obtained from the voltage measured along a transmission line leading to an antenna; the measured value of the maximum voltage amplitude of a standing wave divided by the lowest voltage value (minimum amplitude) of a standing wave yields the value if the voltage standing wave ratio. If there test antenna is not properly matched to the receiver; there will be power reflection, which indicates that the reflection coefficient (Γ) is not zero), thereby resulting to a reflected voltage wave travelling down on the transmission line as a standing waves. In such situation, the voltage along the transmission line should have a constant magnitude and therefore VSWR will be equal to "1" as indicated on the illustration on the figure below:

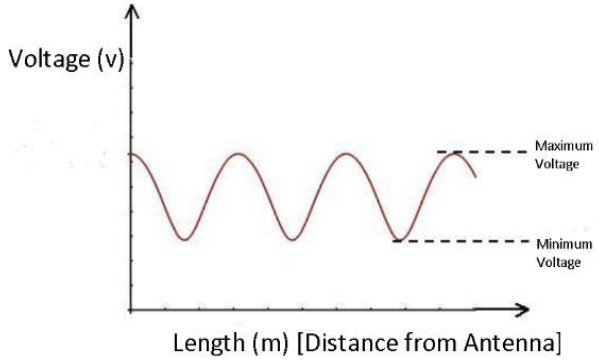

Figure 14: A graph of Voltage (v) Against Length (m) [Measured Along a Transmission Line]

The Voltage Standing Wave Ratio is a function of the return loss also known as the reflection coefficient; indicating the power in decibel reflected from the antenna under test. The voltage standing wave ratio could also be defined mathematically with respect to the reflection coefficient also referred to as S11 parameter or return loss or reflection coefficient as:

$$VSWR = \frac{1 + |\Gamma|}{1 - |\Gamma|}$$

The above equation describes the numerical mapping between the voltage standing wave ratios with the reflected power, reflection coefficient.

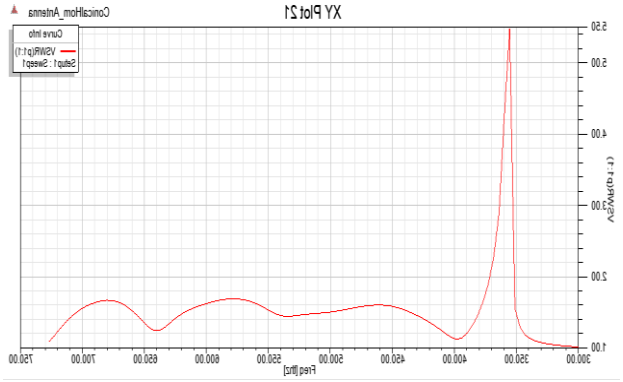

Figure 15: Voltage Standing Wave Ratio for Test Antenna

The VSWR of 5.5 at 360THz indicates that less than 51% of power is wasted with S parameter at maximum of 0.714 and reflected power of -2.92dB. The result of the VSWR within the frequency for visible light spectrum (430THz to 770THz) is very desirable; no power wastage and heat build-up. The maximum VSWR is 1.7:1 ratio indicates small level of back refection occurred within the frequencies of interest and power wastage is less than 10%. The reflection coefficient will be at maximum of 0.3333 and reflected power of -9.55dB.We could summarize that the relationship between voltage standing wave ratios and the mismatch loss, (S11/Gamma); that we could state that the voltage standing wave ratio is always a positive real value for antennas in non-complex antenna setup. The lower the voltage standing wave ratios is best antenna characteristics matched to the transmission line and therefore more power in decibels is delivered to the antenna. An ideal voltage standing wave ratio value and the most minimal value is 1.0; it means that there absolutely no power reflection from the antenna. Since the antenna of interest is to operate from within the visible, light spectrum 430-769 THz the VSWR less than two. It implies that the voltage standing wave ratio is less than 2.0 over the specified frequency range and implies that the reflection coefficient is less than 0.33333 over the aforementioned frequency range. The table below shows the corresponding relationship between voltage standing wave ratio, total reflected power (S11 parameter), and total reflected power. It is important to remember that the percentage reflected power is commonly known as the reflection coefficient (Γ) squared. Table: Voltage Standing Wave Ratio (VSWR), Percentage Reflected Power, and Return loss (S11)

Published By:
Blue Eyes Intelligence Engineering and Sciences Publication (BEIESP)

Table 1: VSWR, Percentage Reflected Power, and Return loss (S11)

VSWR	Return Loss (S11)	Reflected Power (%)	Reflected Power (dB)
1	0	0	-Infinity
1.5	0.2	4	-14
2	0.333	11.1	-9.55
2.5	0.429	18.4	-7.36
3	0.5	25	-6
3.5	0.556	30.9	-5.1
4	0.6	36	-4.44
5	0.667	44	-3.52
6	0.714	51	-2.92
7	0.75	56.3	-2.5
8	0.778	60.5	-2.18
9	0.8	64	-1.94
10	0.818	66.9	-1.74
15	0.875	76.6	-1.16
20	0.905	81.9	-0.87
50	0.961	92.3	-0.35

Let us look at the VSWR spike that occurred at 360THz resulting to a VSWR of 5.5 or approximately a VSWR of six. We could deduce other related characteristics using the above.

At the table above, we could deduce that a voltage standing wave ratio of 6 has 51 percent of power supplied by the receiver reflected from the antenna of about 49 percent of the power is supplied to the antenna; moreover, the reflected power in decibel stands at -2.92dB and S11 parameter of 0.714. It is essential to know that at a reflected power of 0 dB means that 100 percent power (overall) is reflected, whereas -10 dB is equivocal to a 10 percent of power reflection; however, in a situation that all the power is reflected, then the Voltage Standing Wave Ratio will approach infinity. It could be seen as there are minimal difference in terms of the percent-reflected power of 4.2 percent change, if the Voltage Standing Wave Ratio increases from7 to 8; however there is an 11percent difference in terms of the percentage reflected power, when the voltage standing wave ratio changes from the value of 1 to 2. It is important to know that the voltage standing wave ratio is a function of the reflection coefficient (Γ) and not linear in nature. As the antenna exhibits a VSWR less than 2 from 430THz to 720 THz. The antenna is well matched and requires less impedance matching efforts. If the VSWR increase results to two major negative effects such as it increases the level of power reflection from the antenna, which is not transmitted. The other effect is that the reflected power travels back to the to the source of transmission (radio), which in turn could damage the radio and minimise its performance in terms of information or signal integrity.

F. Group Delay

The group delay simulation is used to investigate the overall delay characteristics of circularly polarized lossless stacked of biological materials on the Horn antenna; which is calculated through the derivative of the input phase function frequency without the effect of the second order of the far-field phase achieved in closed loop approach by the HFSS Ansoft pack. It is a function of the test antenna's equivalent Resistor-Inductor- Capacitor-Conductance circuit parameters using the antenna's resistance per unit length (Ω/m), inductance per unit length (H/m), capacitance per unit length (F/m) and conductance per unit length (S/m) transmission line properties.

The maximum group delay of the test antenna displays asymptotic properties with maximum values at input resistance as it rises without clipping. The rate at which this occurs is inversely proportional to the stacking of the materials; therefore, the peak group delay of the stacked structure moves in the direction of $4.3 * 10^{-14} s$ at 350THz as the inductance reduces, and approaches an asymptotic mark as the inductance rises. However, all of characteristics exhibited below by the group delay graph are independent of the test antenna's circular polarization.

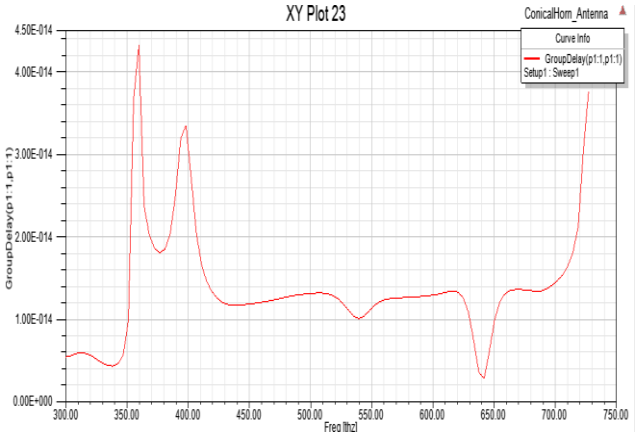

Figure 16: Group Delay against Frequency plot

G. Specific Absorption Ratio (SAR)

The specific absorption ratio (SAR) provides an indication of the measured power absorbed in terms of heat by the biological material in the presence of an electromagnetic field. The quantity of energy dissipated in heat per unit of mass.

$$SAR = c\frac{\partial T}{\partial t}\frac{1}{m}$$

Whereby c is the total specific heat capacity of the material
M is the concentration per milli-litre (ml)

The use of very high frequency electromagnetic fields could damage some of biological tissues over a long period by damaging molecular structure, induced-stress, loss of density and increasing the biological material temperature.

The biological effects of optical frequency field can be evaluated at various levels on HFSS Ansoft including the local specific absorption ratio, the temperature, and loss in volume density measurement.

The aforementioned biological effects from visible light spectrum frequency fields can be classified into three categories namely: high-level effects (thermal defects of bio-optical material), intermediate-level effects (Nano-scale A-thermal defects of bio-optical material), and low-level effects (non-thermal defects of bio-optical material).

Published By:
Blue Eyes Intelligence Engineering
and Sciences Publication (BEIESP)

Thermal effects are energy depositions, which may be partially reduced or controlled to some degree by natural human thermoregulatory capacity. The results of the defects caused by the penetration of the visible light into human eye may result to some alterations to the life span of the rod and cones, morphology, genetic composition and chromosomal morphology and the enzyme activities inside the human eye over a long period.

Local Specific Absorption Ratio Field Plot in W/Kg

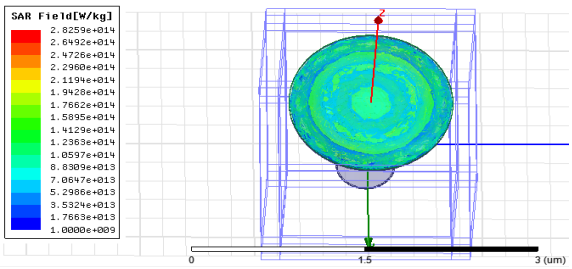

Figure 17: Field plot of Local Specific Absorption Ratio

The internal region shows some evidence of more intense power absorption more than the outer region outside the red annotation. The maximum SAR field intensity on the biological material is at$1.943*10^{14}$ watts per kilogram.

H. The Temperature of the Materials

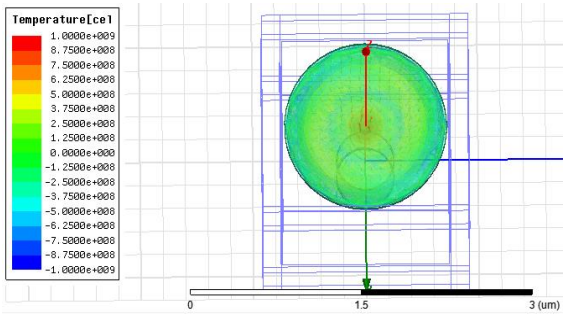

Figure 18: Field Plot of Temperature Distribution on the Biological Material

The result is similar to the above result of local specific absorption ratio as the internal region shows some evidence of more intense temperature at the inner region compared to the outer region outside the red annotation at a maximum of $3.75 *10^{8}$ ce.

I. Volume Loss Density

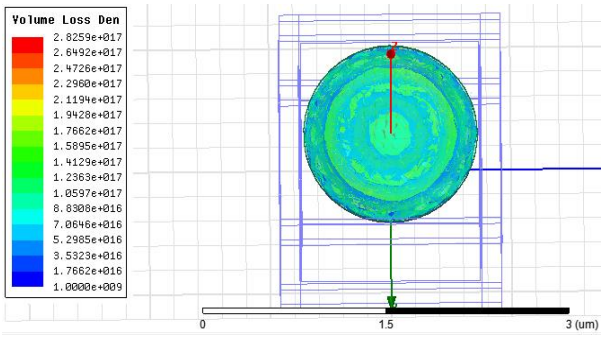

Figure 19: Field Plot of Volume Loss Density on the Biological Material

The result is synonymous with the specific absorption ratio as the internal region shows more evidence of e intense volume loss more than the outer region outside the red annotation at a maximum of $1.94 *10^{17} kg/m^3$. The results for Specific Absorption Ratio, the temperature, volume loss density and E-field strength field plot simulations shown above has been compared and we could state that there are overwhelming evidence of high risk defects as a result of thermal effects. The biological material is not easy to be model and may consist some gel-like content on its tissues stacked in a cascaded fashion and the required level of complex cascading structure to represent the number of layers required for a rod photoreceptor; the entire process may have some level of limitation due to standard phantom models. We could also categorically state that the reflected light down the antenna is sampled by the cascaded structure upon the horn antenna and the intensity indicates the level of light or darkness witnessed by the human eyes with the aid of the rod antenna.

VI. CONCLUSION

We can conclude from the results obtained that the biological material have an excellent characteristics in spreading behaviour resulting to an overall narrow bandwidth as the Farfield return loss is less than -20dB and therefore, we could say that the layers of materials on the horn antenna serves as an absorber to reduce reflections. The specific absorption ratio of the cytoplasm and membrane reveals that the material is not homogenous; the material electrical conductivity, density, volume, permeability, material optical permittivity, volume loss density and the electric field from the plane wave has a direct impact on the level of absorption. It is because of the electromagnetic wave penetration through the cytoplasm and membrane; heat in terms of temperature is generated. This temperature changes could be the source of common eye defects in older people compared to the young. The passitivity plot shows that with increase in frequency the material tries to limit the magnitude of penetration of signals. The simulation result also highlights that the voltage standing wave ratio less than 1.5 from 400THz to 750THz. It can be used as broadband selective absorption and electromagnetic ware reflection synthetic dielectric material for optical applications in the areas of astronomical equipment's, cross-sectional suppresser for radar, plasma generator, and energy conversion from radio frequency into thermal energy in optics and discharge shields and broadband applications. The magnetic field cannot entirely penetrate through the interior horn material in fast alternating field. At constant field with increate in frequency also increase the eddy current. As the conductivity tends towards infinity in a hollowed waveguide, the skin depth will be less at higher frequency due to skin effect; assuming planes infinitely extended in y-z direction. The parameters of the antenna structure have been analysed to obtain the electromagnetic field characteristics. The specific absorption ratio is direct effect of the quantity of electromagnetic measurement at visible light spectrum and finally the electrical properties of rod photoreceptor tissues where described, used in modelling the material parameters such as conductivity and permittivity.

Published By:
Blue Eyes Intelligence Engineering and Sciences Publication (BEIESP)

REFERENCES

1. Daniyan, O.L. et al., (2014). Horn Antenna Design : The Concepts and Considerations. , 4(5), pp.706–708.
2. Sigal, I.A., Flanagan, J.G. & Ethier, C.R., (2005). Factors Influencing Optic Nerve Head Biomechanics. Investigative Opthalmology & Visual Science, 46(11), p.4189 [online] available from <http://iovs.arvojournals.org/article.aspx?doi=10.1167/iovs.05-0541> [13 August 2013].
3. Drago, G.P. & Ridella, S., (1982) Evaluation of electrical fields inside a biological structure. The British journal of cancer. Supplement, 5, pp.215–9 [online] available at: <http://www.pubmedcentral.nih.gov/articlerender.fcgi?artid=2149332&tool=pmcentrez&rendertype> [23 August 2013]
4. Gimsa, J. et al., (1996). Dielectric spectroscopy of single human erythrocytes at physiological ionic strength: dispersion of the cytoplasm. Biophysical Journal, 71(1), pp.495–506.
5. Hoffmann, J. et al., (2009). Comparison of electromagnetic field solvers for the 3D analysis of plasmonic nano antennas. Modeling Aspects in Optical Metrology, p.12. [online] available from < http://arxiv.org/abs/0907.3570> [28 August 2013].
6. Singh, K. & Siwach, A., (2013). Advancement in Designing of Wideband Horn Antenna. , 4(April), pp.719–722.
7. Karpen, J.W. et al., (1988). Gating kinetics of the cyclic-GMP-activated channel of retinal rods: flash photolysis and voltage-jump studies. Proceedings of the National Academy of Sciences of the United States of America, 85(4), pp.1287–1291.
8. Sigal, I.A., Flanagan, J.G. & Ethier, C.R., (2005). Factors Influencing Optic Nerve Head Biomechanics. Investigative Opthalmology & Visual Science, 46(11), p.4189 [online] available from <http://iovs.arvojournals.org/article.aspx?doi=10.1167/iovs.05-0541> [13 August 2013].
9. R, W.P.C.J., Pichon, L. & Razek, A., (2000). A 3D " nite element method for the modelling of bounded and unbounded electromagnetic problems in the time domain. , (April 1999), pp.527–540.
10. Raja, W. et al., (2009). Surface Plasmon Resonance Sensors : Optimization of D iffraction G rating and P rism C ouplers Results : , p.2000.
11. Njoku, C.C. et al., (2012). Simulation Methodology for Synthesis of Antenna Substrates With Microscale Inclusions. IEEE Transactions on Antennas and Propagation, 60(5), pp.2194–2202 [online] available from < https://dspace.lboro.ac.uk/dspace-jspui/handle/2134/9993> [09 August 2013].
12. Nicolson, S.T. & Voinigescu, S.P., (2006). Methodology for simultaneous noise and impedance matching in W-band LNAs. Technical Digest - IEEE Compound Semiconductor Integrated Circuit Symposium, CSIC, (5), pp.279–282 [online] available from <http://ieeexplore.ieee.org/xpls/abs_all.jsp?arnumber=4110041> [08 August 2013].
13. Kazemipour, A. et al., (2014). The Horn Antenna as Gaussian Source in the mm-Wave Domain. Journal of Infrared, Millimeter, and Terahertz Waves, 35(9), pp.720–731 [online] available from < http://link.springer.com/article/10.1007/s10762-014-0077-9\nhttp://link.springer.com/content/pdf/10.1007%2Fs10762-014-0077-9.pdf> [21 August 2013].
14. Tobey, F., L., Enoch, J., M., and Scandrett, J., H., (1975).Experimentally determinded optical properties of goldfish cones and rods. [Online] Available at: www.Iovs.arvojournals.org / [Accessed 3 Aug. 2014].
15. Saade, C., Alvarez-Delfin, K. and Fadool, J. (2018). Rod Photoreceptors Protect from Cone Degeneration-Induced Retinal Remodeling and Restore Visual Responses in Zebrafish. [Online] Available at: https://www.ncbi.nlm.nih.gov/pmc/articles/PMC3711385/ [Accessed 3 Aug. 2014].
16. Ribelayga, C., Cao, Y. and Mangel, S. (2018). The Circadian Clock in the Retina Controls Rod-Cone Coupling. [Online] PMC Journals. Available at: https://www.ncbi.nlm.nih.gov/pmc/articles/PMC5581203/ [Accessed 20 Aug. 2014].
17. Charman, W. N. (1991). 'Optics of the Human Eye'.Visual Optics and Instrumentation, CRC Press, Boca Raton.Pg 1-26.
18. Chen, S., Donoho, D., and Saunders, M. (1998). 'Automatic decomposition by basis pursuit'. SIAM Journal of Scientific Computation 1(3), 33–61
19. Gorodnitsky, I. F., and Rao, B. D., (1997).'Sparse signal reconstruction from limited data using FOCUSS: a re-weighted minimum norm algorithm'. IEEE Transactions on Signal Processing 45(3), 600–616
20. Watson, A. B. and Ahumada, A. J. (1985) 'Model of Human Visual-Motion Sensing'. Optical Society of America, Journal, A: Optics and Image Science 2, 322-342
21. Das, R., (2003). Transmission of Electromagnetic Power Through a Biological Medium. , pp.1–149.
22. Poggio, T., Fahle, M., and Edelman, S. (1991) Fast Perceptual Learning in Visual Hyperacuity
23. Condon, E.U., and Odishaw, H., (1958) 'Handbook of Physics'. McGraw Hill Book Company, Inc. New York Toronto London, 1, 4-119.
24. Fu, Y., (2010). 'Phototransduction in rod and cones'. Medical Educational Website [Online] Available from <http://webvision.med.utah.edu/book/part-v-phototransduction-in-rods-and-cones/phototransduction-in-rods-and-cones/> [28 August 2013]
25. Montag (2015). 'The Eye' Medical Educational Website [Online] Available on http://web.csulb.edu/~cwallis/482/visualsystem/eye.html> [8 July 2014]
26. Smith, S. W. (2011).' Image Formation & Display- Cameras and Eyes'. The Scientist and Engineer's Guide toDigital Signal Processing. [Online] available from <http://www.dspguide.com/ch23/2.htm> [20 June 2014].
27. Hatori, M., and Panda, S., (2015).' The emerging roles of melanopsin in behavioral adaptation to light' Medical Educational Website [Online] available from <http://panda.salk.edu/pdf/emergingrolesofmopn4.pdf > [7 August 2013]
28. Mustafi, D., Engel A., B., Palczewskia, K. (2009).'Structure of cones photoreceptors' Medical Educational Website [Online] Available from <http://pharmacology.case.edu/department/facuity/primary/pages/Palczewski/articles/Progress%20in%20Retinal%20and%20Eye%20Research.pdf> [14 April 2014]
29. Bowmaker, J. K., and Dartnallt, H. J. A., (1979). 'Visual pigments of rods and cones in a human retina'. [Online] Available from <http://www.ncbi.nlm.nih.gov/pmc/articles/PMC1279132/pdf/jphysiol00783-0492.pdf> [14 April 2014].
30. Sinaeur (2001). 'Anatomy of the Human eye'. Medical Educational website [Online]. Available from <http://www.ic.ucsc.edu/~bruceb/psyc123/Vision123.html.pdf>[26 August 2013]
31. Clark, R. N (2009). 'Experiments with Pixels per Inch (PPI) on Printed Image Sharpness'. Available from <http://www.clarkvision.com/articles/printer-ppi>[27 August 2013]
32. Bandung, D., (2013).'Eye diagram and function' [Online] available at <http://diagramreview.com/eye-diagram-and-functions/eye-diagram/> [14 June 2015]
33. Sylvani, O., (2000).' Approximate ranges of vision regimes and receptor regimes' available at <http://www.ecse.rpi.edu/~schubert/Light-Emitting-Diodes-dot-org/chap16/chap16.htm> [17 June 2015].
34. Hajiaboli, A. (2008). 'Light Interaction with Human Retinal Photoreceptor: Finite-Difference Time-Domain Analysis'. Department of Electrical & Computer Engineering, McGill University, Montreal, Quebec H3A 2A7, Canada.
35. Virgina Regional College (2013). 'Muller Cell'. College Educational website [Online] available from <http://www.vetmed.vt.edu/education/curriculum/vm8054/eye/MULLER.HTM > [26 August 2013]
36. Barton, H., and Byrne, K. (2007). 'Introduction to Human Vision, Visual Defects & Eye Tests'.
37. Arora, R.K., Vijayaraghavan, S. & Madhavan, R., (1972). Modes of Propagation in a Coaxial Waveguide with Lossless Reactive Guiding Surfaces. IEEE Transactions on Microwave Theory and Techniques, 20(3), pp.210–214.
38. Iroanusi, K. (2012).'Hyper Acuity derivation of Human Visual System functioning as a Phased Array Antenna'. Coventry University
39. Howard and Roger,(1995)"Seeing in Depth" Porteous and Oxford University Press.
40. Howard and Roger,(2005)"Perceiving in Depth" Porteous and Oxford University Press.

41. Gabriel, C.,(1996) Compilation of the Dielectric Properties of Body Tissues at RF and Microwave Frequencies. , (June) [online] available from http://oai.dtic.mil/oai/oai?verb=getRecord&metadataPrefix=html&identifier=ADA309764> [20 May 2012].
42. Gimsa, J. et al., (1996). Dielectric spectroscopy of single human erythrocytes at physiological ionic strength: dispersion of the cytoplasm. Biophysical Journal, 71(1), pp.495–506.
43. Hajiaboli, A., (2008) FDTD Analysis of Retinal Photoreceptor Outer-Segment : Effect of Stacking Nano-Layers of Membrane and Cytoplasm. , pp.3–6.
44. Karpen, J.W. et al., (1988). Gating kinetics of the cyclic-GMP-activated channel of retinal rods: flash photolysis and voltage-jump studies. Proceedings of the National Academy of Sciences of the United States of America, 85(4), pp.1287–1291.
45. Mustafi, D., Engel, A.H. & Palczewski, K., (2009). Structure of cone photoreceptors. Progress in Retinal and Eye Research, 28(4), pp.289–302 [online] available from <http://dx.doi.org/10.1016/j.preteyeres.2009.05.003> [07 August 2013].

AUTHOR PROFILE

Kennedy A. Iroanusi , Kennedy Iroanusi is currently a Lecturer at Dudley College of Technology, teaching Electrical and Electronics Engineering related units. He studied Electrical and Electronics Engineering at University of Birmingham and carried out some research at Coventry University. He formerly worked at Coventry University and aim to complete a PhD by publication at Warwick University. Whilst at Coventry University; I lectured undergraduates on Analogue and Digital Electronics, Electrical Engineering module, Very Speed Hardware Description Language (VHDL) both at Undergraduate and post graduate students, Digital Signal Process (DSP) and communication. He has a keen interest in Analogue and Digital Electronics, Electrical Engineering and Microprocessor, Human Visual systems, Car security products, high-speed digital processing solutions, Microwave systems, Antenna design, Radio Frequency (RF) subsystem, , Field programmable gate array (FPGA) or Complex Programmable Logic Device (CPLD) prototyping, application specific integrated circuits (ASIC),System on Chip (SOC), Verification, Mixed Signals (Digital and Analogue).

Published By:
Blue Eyes Intelligence Engineering and Sciences Publication (BEIESP)